Chemical and Structural Factors Governing Transparent Conductivity in Oxides

B.J. INGRAM, G.B. GONZALEZ, D.R. KAMMLER,* M.I. BERTONI & T.O. MASON

Department of Materials Science and Engineering and Materials Research Center, Northwestern University, Evanston, IL 60208, USA

Abstract. The history, applications, and basic requirements of transparent conducting oxides (TCOs) are reviewed. Four basic families of TCOs are recognized, including n-type oxides with tetrahedrally-coordinated cations (e.g., ZnO), n-type oxides with octahedrally-coordinated cations (e.g., CdO, In_2O_3, SnO_2, and related binary and ternary compounds), p-type oxides with linearly-coordinated cations (e.g., $CuAlO_2$, Cu_2SrO_2, and related compounds), and n-type oxides with cage structures (e.g., $12CaO \cdot 7Al_2O_3$). TCO behavior is discussed with attention to structural and chemical factors, especially point defect chemistry, governing carrier generation and transport properties.

Keywords: transparent conducting oxide (TCO), electrical conductivity, point defects, transport

1. Introduction

Transparent conducting oxides, hereafter abbreviated as TCOs, have been known for more than a century. Cadmium oxide was synthesized and characterized in bulk form as early as 1902 [1], with the first thin film work five years later [2]. The first TCO patent for SnO_2 films was filed in 1931 [3], and for SnO_2-based films on glass in 1942 [4]. Such films were employed as aircraft winshield de-icers in World War II [5]. The following decades saw the development of In_2O_3-based TCOs, including indium-tin oxide (ITO) [6], and ZnO-based TCOs, with the first Al-doped ZnO films reported [7] in the same year (1971) as the first ZnO-based varistor [8]. Since that time, there has been steady improvement in the deposition and properties of SnO_2, In_2O_3, and ZnO films, with typical conductivities approaching asymptotic values of ~2500 S/cm for doped SnO_2 and ~10,000 S/cm for doped In_2O_3 and ZnO [9]. The last decade has seen the development of complex TCOs, including binary [9–11] and ternary [12] oxides, and ternary solid solutions [13]. The first copper-based p-type TCO, $CuAlO_2$, was reported in 1997 [14] and a UV-activated, hydrogen-doped TCO based upon the

compound $12CaO \cdot 7Al_2O_3$, was reported just recently [15].

The two largest uses of TCOs are for low-emissivity architectural windows (SnO_2-based films on glass) and as transparent front electrodes in flat panel displays (usually ITO-based films on glass). Gordon [5] gives an extensive overview of TCO applications, including solar cells, electrochromic windows and mirrors, defrosting windows, oven windows, static dissipation, touch-panel screens, electromagnetic shielding, invisible security circuits, etc. More recently, TCOs have been employed in organic light-emitting diodes. With further development of p-type TCOs, all-transparent oxide electronics may be realized; transparent p-n junctions have already been demonstrated [16].

The basic requirements for TCOs can be described with respect to the simplified band structure diagrams of Fig. 1(a) and (b) (after Hamberg and Granqvist [17]). The first requirement is a host oxide with a band gap in excess of 3.1 eV. Smaller band-gap hosts can be used, relying upon the well-known Burstein-Moss shift with doping to increase to the effective optical gap to greater than 3.1 eV (see Fig. 1(b)). More importantly, there can be no interband transitions less than 3.1 eV in energy. This limits consideration to cations with filled d-shells, such as $3d^{10}$ Cu^+, Zn^{2+} and Ga^{3+} and $4d^{10}$ Ag^+, Cd^{2+}, In^{3+} and Sn^{4+}. These criteria ensure visible

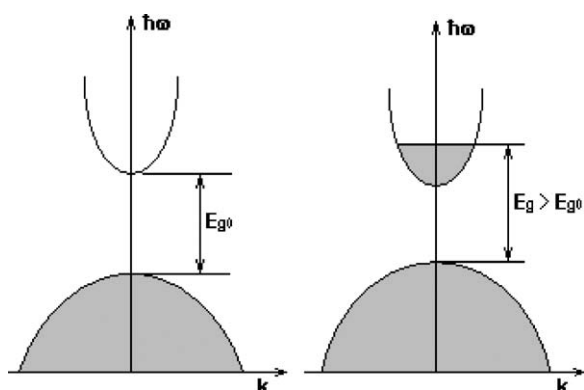*Present address: Sandia National Laboratories, Albuquerque, NM 87185, USA.

Fig. 1. Schematic band structure of undoped and donor-doped transparent conducting oxides (after [17]).

transparency, but not conductivity. The third TCO requirement is the ability to degenerately dope the oxide hosts with carrier contents in excess of 10^{20} cm^{-3}. But carrier content alone does not guarantee high electrical conductivity. The final requirement is a highly dispersed conduction band (for n-types) or valence band (for p-types), leading to high electron or hole mobilities.

Leading TCO materials are n-type and possess electrical conductivities of approximately 10^4 S/cm [9]. Carrier contents tend to be in the 10^{20} to 10^{21} cm^{-3} range, consistent with their highly degenerate character. They exhibit optical absorption coefficients less than 0.10 (often less than 0.05) [5] and as thin films (<1 μm thick), they are more than 80% transparent throughout the visible spectrum. Additional comments regarding doping mechanisms and carrier mobilities are given below.

Existing TCOs can be classified into families by structure, as shown in Table 1. The first family has cations tetrahedrally coordinated by oxygen (Fig. 2(a)), and is n-type in character. ZnO is the only known oxide to possess this coordination exclusively. The

Table 1. Families of transparent conducting oxides.

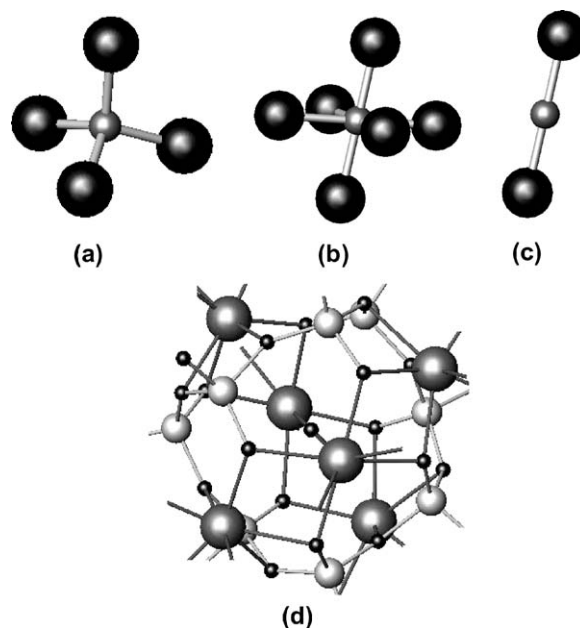| Structural feature	Carrier type	Examples
Tetrahedrally-coordinated cations	n-type	ZnO
Octahedrally-coordinated cations	n-type	CdO, In$_2$O$_3$, SnO$_2$, CdIn$_2$O$_4$, Cd$_2$SnO$_4$, etc.
Linearly-coordinated cations	p-type	CuAlO$_2$, SrCu$_2$O$_2$, etc.
Cage framework	n-type	12CaO·7Al$_2$O$_3$

Fig. 2. Schematic representation of cation coordination in (a) tetrahedral family of TCOs, (b) octahedral family of TCOs, (c) linear family of TCOs, and (d) cage structure TCOs. In Figs. (a) through (c), the small balls are cations and the large balls are oxygen anions. In Fig. (d), the large dark balls are Ca ions, the light gray balls are Al ions, and the small dark balls are oxygen anions. Note that only one of 12 cages in the unit cell of mayenite (12CaO·7Al$_2$O$_3$) is represented in Fig. (d).

second family has cations in octahedral coordination (Fig. 2(b)), and is also n-type in character. This is the largest family of TCOs, including CdO, In$_2$O$_3$, SnO$_2$, CdIn$_2$O$_4$, Cd$_2$SnO$_4$, and most of the best n-type complex oxide materials. The third family of TCOs has cations in linear coordination with oxygen (Fig. 2(c)), and is p-type in character. This family includes CuAlO$_2$ and related Cu- and Ag-based delafossites (see below for a description of the structure) plus SrCu$_2$O$_2$. Finally, the recent cage-structure oxide, 12CaO·7Al$_2$O$_3$ (one cage is shown in Fig. 2(d)), is listed as the first member of a potential new family of TCOs; it is n-type in character. We have not included p-type ZnRh$_2$O$_4$ in our classification, due to its relatively small band gap [18].

In what follows, point defect reactions are written in Kröger-Vink notation. Each point defect entity can be represented as M_s^c, where M stands for the particular species (atom, vacancy, electron, etc.), s stands for its site (i stands for interstitial, and there is no "site" for electronic species), and c stands for the effective charge of the species relative to the neutral, defect-free lattice

($'$ represents negative charge and $\cdot$ represents positive charge).

## 2. The Tetrahedral Cation Family of *n*-Type TCOs

Zinc oxide is the only simple oxide with all its cations in tetrahedral coordination (Fig. 2(a)). It possesses the wurtzite crystal structure. ZnO can be readily donor doped by intrinsic defects, and by extrinsic doping with cations (Al^{3+}, Ga^{3+} or In^{3+}) or anions (F^-). However, *p*-type doping has proved exceedingly difficult to date, certainly to the levels ($>10^{20}$ cm^{-3}) required of transparent conductors.

Tetrahedral Zn and Cd cations exist in other structures, for instance in spinels such as Zn_2SnO_4, Cd_2SnO_4 and $CdIn_2O_4$, and in the homologous series of compounds with stoichiometry, $kZnO \cdot In_2O_3$ ($n = $ 3–9, 11, 13, etc.) [19]. However, we have shown that Zn in tetrahedral coordination in the spinel structure does not contribute significantly to overall conductivity, presumably due to the much larger Zn-Zn distance in spinels vs. that in wurtzite [20]. And in both the spinel structure and the layered homologous series of compounds, other cations (e.g., In or Sn) when present in octahedral coordination tend to dominate transport [19, 20]. For example, conductivity increases monotonically with decreasing k in $kZnO \cdot In_2O_3$ ($n = $ 3–9, 11, 13, etc.) to values characteristic of undoped In_2O_3 prepared under identical conditions [19].

Although the tetrahedral cation family of TCOs appears to be limited to ZnO, much has been learned from the composition-structure-property relationships in this material, which can be readily extended to the octahedral family of TCOs (discussed below). For example, Gordon [5] has been able to estimate an upper limit for electron mobility, based upon the contributions of phonon scattering ($\sim$250 cm^2 V^{-1} S^{-1} at low doping levels, $\sim$10^{16} cm^{-3}, in ZnO), ionized impurity scattering ($\sim$90 cm^2 V^{-1} S^{-1} at $>10^{20}$ cm^{-3} [9]), and grain boundary scattering ($\sim$200 cm^2 V^{-1} S^{-1} [9]). The contribution due to grain boundary scattering is controversial, with some experts discounting any contribution from grain boundaries at such high levels of degenerate doping [20]. Nevertheless, the estimate arrived at, 50–66 cm^2 V^{-1} S^{-1}, agrees well with values obtained for optimized ZnO-based films, with best practice conductivities approaching 1×10^4 S/cm [9].

3. The Octahedral Cation Family of *n*-Type TCOs

TCO-active cations in octahedral coordination (Fig. 2(b)) distinguish the largest family of TCOs, including the technological workhorse materials—ITO (Sn-doped In_2O_3) and doped SnO_2. We recently reported the equilibrium subsolidus phase diagram for the CdO-In_2O_3-SnO_2 system at 1175°C in air, produced by standard solid state reaction technique [21]. This diagram is reproduced in Fig. 3. Each of the end members is an outstanding *n*-type TCO when appropriately donor-doped. The prevailing intrinsic donor defect in the pure oxides is thought to be oxygen vacancies, according to the reaction [22]:

$$O_O^x \Leftrightarrow \frac{1}{2}O_2(g) + V_O^{\cdot\cdot} + 2e' \qquad (1)$$
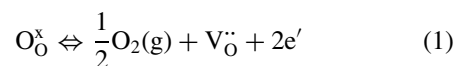
However, aliovalent donor-doping is a much more effective means of carrier generation. Although not reflected on the phase diagram (we detected bulk solubilites of 1.5% or less for In_2O_3 in CdO and 1% or less for SnO_2 in CdO [22]), CdO can be successfully donor-doped by In^{3+} or Sn^{4+} substitution for Cd^{2+}, especially in thin films, leading to high conductivities [23]. It is similarly well known that In_2O_3 can be donor-doped (by Sn^{4+}), as reflected in the In_2O_3-SnO_2 binary (see Fig. 3), which yields the well known ITO material. In contrast, acceptor-doping of the end members is limited in extent. We detected bulk solubilities of 1% or less for CdO in In_2O_3 and similar levels for CdO or In_2O_3 in SnO_2. Furthermore, these acceptor-doped compositions were highly resistive, albeit *n*-type in character. This is attributable to ionic compensation of the acceptors by oxygen vacancies, i.e., $[V_O^{\cdot\cdot}] = \frac{1}{2}[A']$, with an associated decrease of the electron population according to the defect reaction in Eq. (1). To the authors' knowledge, none of the phases in the octahedral cation family have been successfully rendered *p*-type in character.

The defect structures of the donor-doped end-members may be more complex than just described (i.e., simple aliovalent doping). As early as 1982, it was hypothesized that high levels of tin doping in thin films of ITO lead to the formation of neutral associates, including $(2Sn_{In}^{\cdot} O_i'')^x$ and other non-reducible clusters of similar stoichiometry [24]. The bixbyite structure of In_2O_3 is derived from the fluorite structure, with one fourth of the oxygens removed. These so-called
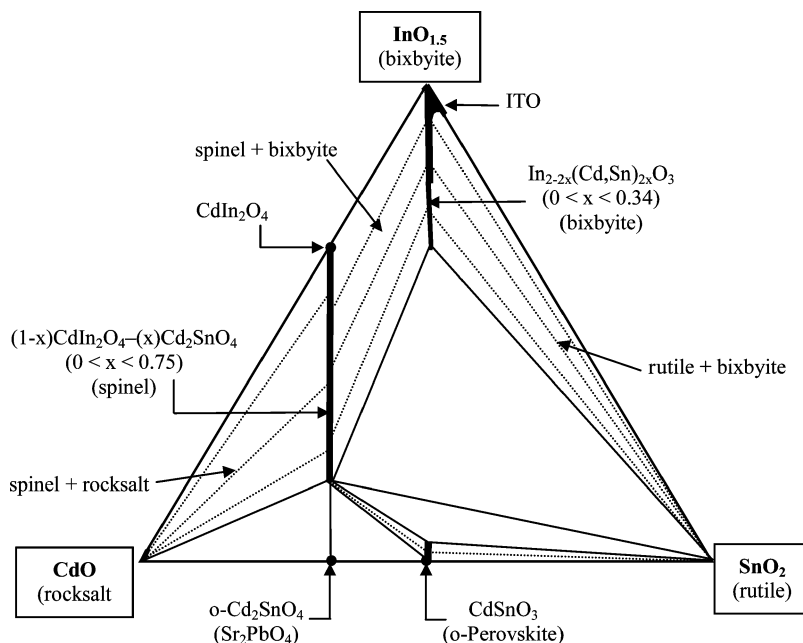
Fig. 3. Subsolidus phase diagram for the $CdO-In_2O_3-SnO_2$ system at $1175°C$ in air (from [21], used with permission).

"structural vacancies" are actually empty interstitial positions. As such, the defect associates/clusters proposed by Frank and Köstlin [24] are quite feasible. Furthermore, it is well known that hydrogen-reduction subsequent to initial processing greatly enhances the electron populations. According to the Frank and Köstlin model, hydrogen reduction removes the oxygen from the reducible $(2Sn_{In}^{\cdot} O_i'')^x$ species, freeing the Sn species to act as donors, according to:

$$(2Sn_{In}^{\cdot}O_i'')^x \Leftrightarrow \frac{1}{2}O_2(g) + 2Sn_{In}^{\cdot} + 2e' \qquad (2)$$
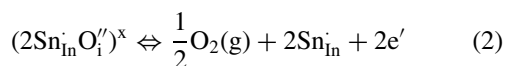
We recently confirmed the existence of significant concentrations of oxygen interstitials in as-fired and quenched ITO specimens by combined Rietveld analysis of powder X-ray diffraction and neutron diffraction patterns [25]. This work was carried out at the Advanced Photon and Intense Pulsed Neutron Sources at Argonne National Laboratory. The analyses confirmed the presence of oxygen interstitials in significant amounts. More importantly, the ratio of Sn-donors to oxygen interstitials was ~2:1, in agreement with the Frank and Köstlin associate. Furthermore, EXAFS measurements at the In-edge showed In-O distances in as-fired and quenched ITO to be virtually identi-

cal to those in undoped In_2O_3 (~0.218 nm), whereas EXAFS measurements at the Sn-edge showed Sn-O distances to be much smaller (~0.207 nm). These data provide strong support for the existence of Sn-oxygen interstitial defect associates in ITO. Furthermore, hydrogen reduction (4% H_2/96% N_2) for 6 h at $500°C$ did not remove all of the oxygen interstitials, thereby substantiating the presence of non-reducible higher order associates.

It may prove that such associates and higher order clusters play a more important role in the doping of TCOs than originally thought. As commonly observed in thin films [23], an initial linear regime (electron population increasing linearly with doping level) is usually followed by saturation (electron population unchanged with further doping), and can even be followed by a regime of decreasing electron concentration at higher doping levels, without any indication of a second phase being precipitated. Such behaviors are suggestive of neutral associates and higher order clusters, as described above. It should also be stressed that the reducible associate in ITO plays the dominant role during hydrogen-reduction, i.e., that the reaction of Eq. (2) (reduction of associates) dominates over the reaction of Eq. (1) (formation of oxygen vacancies) during the reduction process. This is an important finding in that

most TCOs are subjected to a post-processing reduction anneal (to enhance electrical conductivity) prior to their use as transparent electrodes.

The additional phases in the CdO-In$_2$O$_3$-SnO$_2$ system are similarly good-to-excellent TCOs. Except for orthorhombic Cd$_2$SnO$_4$ phase (Sr$_2$PbO$_4$ structure), the other phases—the distorted orthorhombic CdSnO$_3$ phase (perovskite structure), the CdIn$_2$O$_4$-Cd$_2$SnO$_4$ solid solution (spinel structure) and the co-doped In$_{2-2x}$Cd$_x$Sn$_x$O$_3$ phase (bixbyite structure)—exhibit extended solid solubilities. These appear as vertical lines on the phase diagram (Fig. 3). This is attributable to the substitutions being isovalent and nearly size-matched in character. For example, the co-substitution of bixbyite by cadmium and tin involves the replacement of two In^{3+} species by one divalent (Cd^{2+}) and one tetravalent (Sn^{4+}) species. In Kröger-Vink notation, there is a balance of donors and acceptors, as reflected by the replacement reaction:

$$CdO + SnO_2 + 2In_{In}^x \Leftrightarrow Cd'_{In} + Sn_{In}^{\cdot} + In_2O_3 \quad (3)$$
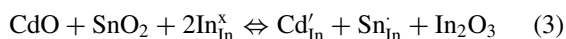
The identical reaction also holds for the CdIn$_2$O$_4$-Cd$_2$SnO$_4$ solid solution. Furthermore, the average of the Cd^{2+} and Sn^{4+} radii in octahedral coordination (0.095 nm and 0.069 nm, respectively) or 0.082 nm is very close to that of octahedral In^{3+} (0.080 nm) [26]. As we have pointed out previously, these extended solid solubilities offer the opportunity for "band structure engineering," similar to the practice in compound semiconductors. In other words, the band edges and fundamental gap (see Fig. 1(a)) can be modified independently of doping-induced changes, i.e., due to the Burstein-Moss shift (Fig. 1(b)).

What is intriguing about the solid solution phases in the CdO-In$_2$O$_3$-SnO$_2$ system is that it is impossible to prepare them in an undoped state, i.e., at low carrier concentrations. This is surprising, given the isovalent co-substitution mechanism described above and in Eq. (3), with a balance of donors and acceptors (i.e., fully compensated). Instead, we have demonstrated the trend in each of these materials toward an inherent excess of donors to acceptors, such that $n = [Sn_{In}^{\cdot}]$– $[Cd'_{In}]$. This has been observed in both bulk [21] and thin film materials [27]. Wei and Zhang [28], using a first-principles band structure method, determined the relative energetics for Sn-on-Cd antisite defects in Cd$_2$SnO$_4$, and concluded that these were energetically favored over other defects, including oxygen vacancies. What is significant about these findings is that these
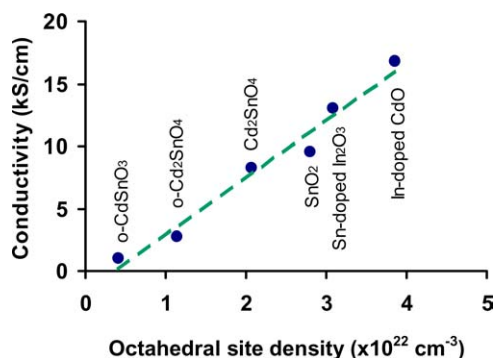

Fig. 4. Conductivities for the various phases in the CdO-In$_2$O$_3$-SnO$_2$ system vs. the density (cm^{-3}) of octahedrally coordinated cations (from various sources, see text).

appropriately co-substituted phases are "self-doped" TCOs, i.e., they require no reduction anneal in order to enhance their electron populations. Furthermore, they are "robust" TCOs in that they should be relatively immune to the various redox steps required in the processing of microelectronic and opto-electronic devices.

As early as 1977, Shannon et al. [29] argued that "continuous edge sharing of Cd^{2+}, In^{3+} and Sn^{4+} octahedra is a necessary criterion for the formation of a transparent conductor." We would only modify this statement to allow for corner sharing of octahedra, as in the case of orthorhombic CdSnO$_3$, which is also a TCO. To test the Shannon criterion, we have plotted the "best value" literature conductivities to date for the various phases in the CdO-In$_2$O$_3$-SnO$_2$ system vs. the density (cm^{-3}) of octahedrally coordinated cations (Cd^{2+}, In^{3+} and/or Sn^{4+}) in Fig. 4. The value for the distorted orthorhombic perovskite (CdSnO$_3$) is taken from two sources, one bulk [29] and one thin film [30]. The value for orthorhombic Cd$_2$SnO$_4$ is for a bulk specimen, corrected for porosity [21]. The values for Cd$_2$SnO$_4$ [31], Sn-doped In$_2$O$_3$ [32] and In-doped CdO [33] are for thin film materials. There is no appropriate donor dopant for SnO$_2$ in the CdO-In$_2$O$_3$-SnO$_2$ system, however it is well known that SnO$_2$ can be donor-doped by cations (e.g., Sb^{5+}) or anions (e.g., F$^-$). The value shown in Fig. 4 is from the compilation by Minami [9].

The linear variation of "best" or optimized conductivity with octahedral cation density in Fig. 4 is significant. As pointed out by Gordon [5], the effective mass is very nearly the same ($m^* \sim 0.3m$) in all the best TCO materials, citing results for ZnO, SnO$_2$ and spinel Cd$_2$SnO$_4$. This also holds for CdO [34]. Furthermore, Gordon provides an upper estimate for electron

mobility in highly degenerate TCOs of $\sim$66 cm^2 V^{-1} s^{-1}, based upon phonon and ionized impurity scattering contributions. Values in the 50–70 cm^2 V^{-1} s^{-1} range are routinely observed for optimized *n*-type TCOs [5]. This suggests that the trend in Fig. 4 has to do with the density of states and the corresponding carrier contents in the optimized materials. In other words, the best TCOs in the octahedral cation family are structures with the highest concentrations of octahedral species. By this criterion, the rocksalt structure is best (e.g., CdO), followed by bixbyite (e.g., In$_2$O$_3$) and rutile (e.g., SnO$_2$). The other structures dilute the octahedral species by introducing other cation sublattices/coordinations (e.g., spinel, Sr$_2$PbO$_4$ and perovskite).

For benchmarking purposes, the best TCO conductivities reported to date are in the 15,000–20,000 S/cm range (for In-doped CdO on glass substrates by MOCVD) [33] and $\sim$40,000 S/cm (for epitaxial CdO on MgO substrates by PLD) [23], although the latter films had band gaps slightly less than 3.0 eV.

4. The Linear Cation Family of *p*-Type TCOs

The problem with obtaining *p*-type TCO behavior has to do with the strong localization of holes to oxygen ions at the valence band edge, due to the large electronegativity of oxygen. Kawazoe et al. [16] proposed the use of d^{10} Cu$^+$ or Ag$^+$ cations, whose energy levels should be comparable to that of the 2p^6 electrons on the oxygen ions. Crystal structures were selected from the literature, which have cations in linear (or dumbbell) coordination (Fig. 2(c)) and oxygen ions in pseudo-tetrahedral coordination, to enhance covalency in the cation-oxygen bonding. One such structure is ABO$_2$ delafossite, consisting of stacked layers of O-A$^+$-O dumbbells and edge-shared B^{3+}O$_6$ octahedra. The first such *p*-type TCO was CuAlO$_2$ [16], but any number of B-site cations can be substituted for Al (e.g., Sc, Y, La, Pr, Nd, Sm, Eu, etc.).

By conventional solid state reaction of constituent oxides under moderately reducing conditions, we have synthesized CuAlO$_2$, pure and Mg-doped CuScO$_2$, and pure and Ca-doped CuYO$_2$, employing B-site doping in an attempt to acceptor-dope these materials. The doped CuScO$_2$ and CuYO$_2$ were actually over-doped (at the 5 cation% level) to achieve the maximum solubility in the parent phase; impurity phases were detected in their X-ray diffraction patterns. Under no conditions could
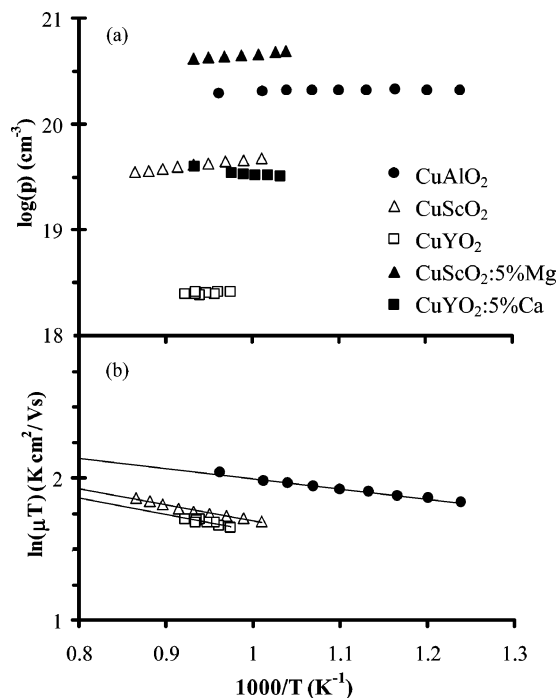
Fig. 5. Electrical property-derived (a) hole contents (assuming small polaron conduction, see text) and (b) mobilities for undoped and doped Cu-based delafossites.

CuAlO$_2$ be intentionally acceptor-doped to any detectable amount, in agreement with the prevailing literature for this material. Bar-shaped specimens were cut from sintered pellets and subjected to in situ electrical property measurements (conductivity, Seebeck coefficient) in a four-probe/thermocouple apparatus at moderate temperatures (500–900°C). It must be stressed that stability ranges for these phases are quite narrow, both in pO$_2$-space and in temperature, and vary from compound to compound.

The electrical properties of the delafossites studied are shown in Figs. 5(a) and (b). The hole content data in Fig. 5(a) have been converted from the experimental Seebeck coefficients (Q) by the standard small polaron formula [35]:

$$Q = k/e[2(1 - c)/c + \text{const}] \qquad (4)$$

where k is Boltzmann's constant, e is the charge of an electron, and c is the fraction of Cu sites occupied by holes (i.e., Cu^{2+}). The small polaron character of the delafossites at elevated temperature is well attested to in the literature [16, 36, 37 and references

therein], in which case the constant in Eq. (4) can usually be neglected. Whereas hole contents are either constant or slightly decreasing with increasing temperature, the conductivities (and therefore the mobilities) are clearly activated. Figure 4(b) plots the resulting mobility-temperature products vs. inverse temperature according to the relation:

$$\mu = (\mu_o/T)\exp(-E_H/kT) \qquad (5)$$

where μ is mobility, T is absolute temperature, E_H is the hopping energy, and μ_o is a pre-exponential factor. It would seem that these materials are members of the same family, with a common value of μ_o (log $\mu_o \sim 2.86$, or $\mu_o \sim 725$ cm^2 V^{-1} s^{-1}). This would set the upper limit for room temperature mobility on the order of 0.1 cm^2 V^{-1} s^{-1} (for $E_H \sim 0.1$ eV). (It should be noted that Hall coefficients are difficult to make and interpret for small polaron materials [38].)

The other factor governing conductivity is the hole content, shown in Fig. 4(a). The relatively high hole content in undoped CuAlO$_2$ ($\sim 10^{20}$ cm^{-3}), at least an order of magnitude higher than tramp impurity levels (by chemical analysis) is difficult to explain. Recently, Shahriari and Poeppelmeier reported Rietveld analyses of neutron diffraction data on hydrothermally synthesized CuAlO$_2$ [39]. They found significant substitution of Al on Cu sites, with a concomitant increase of oxygen intersititials in the Cu-planes in a ratio of 1:2 (Al/O$_i$). They proposed the formation of a charged complex, $(Al_{Cu}^{\cdot\cdot}2O_i'')''$, with aluminum in local fourfold coordination. Furthermore, this cluster acts as an acceptor rather than a donor, thereby increasing the hole population. The fact that hole contents are successively smaller in undoped CuScO$_2$ and CuYO$_2$ is due to the increasing size of the B-site cation, which is therefore less likely to substitute for Cu. We hasten to add that recent first principles calculations of point defects in the delafossite structure suggested that copper vacancies may also be energetically favorable [40]. Such defects are responsible for hole generation in the analogous oxide, Cu$_2$O [41]. Therefore, the presence of copper vacancies cannot be ruled out in the undoped materials.

In larger B-cation compounds, aliovalent substitution becomes a distinct possibility. For example, with acceptor-doping both CuScO$_2$ and CuYO$_2$ increase in carrier content. The Mg-doped CuScO$_2$ exhibits a hole content corresponding to approximately 1% of Cu sites being occupied by holes (Cu^{2+}). We were able to con-

firm a solubility limit (by lattice parameter measurements and the extent of Vegard's law behavior) of approximately 1% Mg substitution for Sc, in excellent agreement with the hole content by Seebeck coefficient analysis, i.e., $p = [Cu_{Cu}^{\cdot}] = [Mg_{Sc}']$. We were unable to detect the solubility limit for Ca in CuYO$_2$, but would estimate this to be less than 0.3%, based upon the Seebeck data.

Finally, whereas CuAlO$_2$ showed a hole content essentially independent of pO$_2$ ($m \sim 0.03$ in $p \sim pO_2^m$) at elevated temperature, CuScO$_2$ and CuYO$_2$ had small but detectable pO$_2$-dependencies ($m = 0.07$ and 0.10, respectively, not shown), which are indicative of p-type behavior with increasing contribution of free oxygen interstitials (as opposed to those bound in associates) according to:

$$\frac{1}{2}O_2(g) \Leftrightarrow O_i'' + 2h^{\cdot} \qquad (6)$$
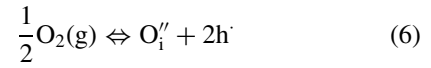
The absence of a pO$_2$-dependence in CuAlO$_2$ is believed to be due to there being insufficient room for isolated oxygen interstitials in the structure [42].

In summary, the prevailing acceptor point defects in the copper delafossites appear to be aliovalent impurities, donor-interstitial associates, and oxygen interstitials. This would result in the electroneutrality condition:

$$p = m[A_B^{m'}] + 2[(Al_{Cu}^{\cdot\cdot}2O_i'')''] + 2[O_i''] \qquad (7)$$

where m is the effective charge of a B-site acceptor. In CuAlO$_2$, the first and third terms are lacking due to the small size of its B-cation (Al) and oxygen interstitial sites, and the middle term is believed to prevail. In large B-site materials, such as CuScO$_2$ and CuYO$_2$, the middle term is unlikely, due to the size mismatch with the copper site, however the first term can be used to advantage. It is also well know that post-processing oxygen treatments can also be used to boost the hole content in the large B-cation materials, most likely associated with enhancing the third term in Eq. (7).

Regardless of defect mechanism, the delafossites are not likely to see substantial improvements in their TCO properties. We can estimate the upper limit for room temperature conductivity, based upon the abovementioned limit for mobility (~ 0.1 cm^2 V^{-1} s^{-1}) and an optimistic doping level of 5% Cu^{2+} ($\sim 10^{21}$ cm^{-3}). The obtained value of ~ 15 S/cm is comparable to the best values obtained to date in thin film delafossite specimens [36, 43].
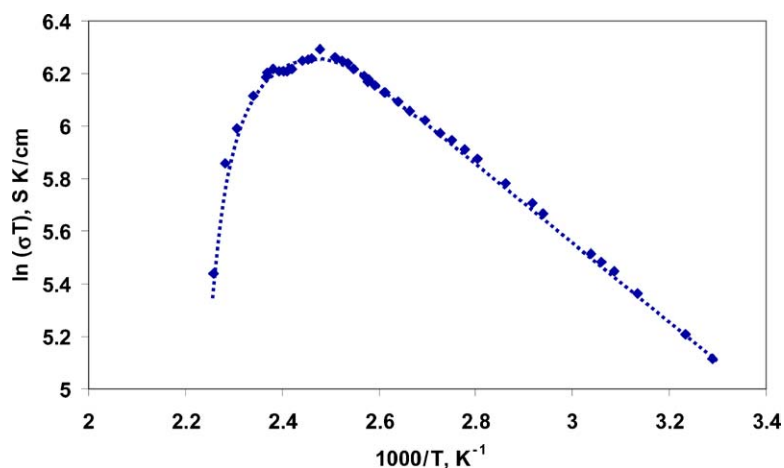
Fig. 6. Electrical conductivity of bulk UV-irradiated, hydrogen-doped $C_{12}A_7$ from room temperature up to $\sim 170^\circ C$.

5. Cage Structure TCOs

Hayashi et al. [15] recently reported the successful conversion of a wide-band gap oxide into a "persistent" *n*-type transparent conductor through hydrogen-doping and subsequent UV-radiation at room temperature. The oxide in question is $12CaO \cdot 7Al_2O_3$ (hereafter referred to as $C_{12}A_7$) which possesses a cage structure (Fig. 1(d)) with two formula units and 12 cages per unit cell, and can be represented as $[Ca_{24}Al_{28}O_{64}]^{4+}$ (the cage framework) plus $2O^{2-}$ (free oxygen ions) in two of the 12 cages. The material can be readily hydrogen-doped at elevated temperatures, followed by quenching, with no apparent change in electrical properties. Upon UV-radiation at room temperature, however, the highly resistive material is rendered conductive, with values on the order of 0.3 S/cm [15]. Furthermore, the conductivity is "persistent," i.e., temperature can be cycled up and down to some maximum use temperature ($240^\circ C$ in the Hayashi et al. work [15]) without being lost.

We have reproduced the Hayashi et al. single crystal and thin film work [15] in bulk and powder specimens. The host $C_{12}A_7$ material was prepared by solid state reaction of high purity constituent oxides in air at $1200^\circ C$. Once phase-purity was confirmed by X-ray diffraction, pellets were pressed and sintered (also at $1200^\circ C$ in air), followed by hydrogen treatment at $1300^\circ C$ (under 4% H_2/96% N_2 at 1 atm) and quenching to room temperature (under H_2/N_2 atmosphere). As-fired and quenched, the specimens were white and insulating. Upon UV-irradiation (with a mercury arc lamp, 20 mW/cm^2 for

40 min), a green surface layer on the order of 15 μm thickness was obtained. We determined the conductivity of this layer to be ~ 0.6 S/cm by four-point conductivity measurements. Loose hydrogen-treated and quenched powders were similarly UV-irradiated to a uniform green color. Their conductivity, determined by the newly developed "powder-solution-composite" method [44] was of the same order of magnitude as the bulk specimens.

Figure 6 shows the electrical conductivity of UV-irradiated, hydrogen-doped $C_{12}A_7$ from room temperature up to $\sim 170^\circ C$. Over this range the Seebeck coefficient is negative (*n*-type), but essentially constant (constant carrier content), confirming the presence of an activated mobility with an activation energy of ~ 0.12 eV. In contradistinction to the Hayashi et al. results on single crystals and thin films [15], the conductivity of our bulk specimens degrades irreversibly above $130^\circ C$. Furthermore, we found it impossible to restore the conductivity of specimens heated above $130^\circ C$ by re-irradiating them with UV light. Our interpretation is that hydrogen is being irreversibly lost above $130^\circ C$.

The specific point defects and carrier transport path(s) in $C_{12}A_7$ are subjects of ongoing study. Whether or not $C_{12}A_7$ remains a lone example or becomes the first of a new family of cage-structure TCOs remains to be seen. As with the delafossites, the small polaron character of transport will limit the achievable conductivity (due to low mobility), regardless of how high a level of carrier doping can be obtained. Nevertheless, the potential for UV-writeable TCOs remains

a compelling argument for additional research and development.

[*Added Note*: During the writing of this paper, the authors became aware of the more recent work of Matuishi et al. [45], who annealed $C_{12}A_7$ crystals with excess calcium in sealed ampoules in order to remove the two free oxygen ions per unit cell. The additional electrons (to maintain charge balance) resulted in room temperature conductivity on the order of 100 S/cm at room temperature, however the crystals thus treated became opaque.]

Acknowledgments

References

1. F. Streintz, *Ann. Phys. (Leipzig)*, **9**, 854 (1902).
2. K. Badeker, *Ann. Phys. (Leipzig)*, **22**, 749 (1907).
3. J.T. Littleton, U.S. Patent 2,118,795 (1938).
4. H.A. McMaster, U.S. Patent 2,429,420 (1947).
5. R.G. Gordon, *MRS Bull.*, **25**, 52 (2000).
6. M.J. Zunick, U.S. Patent 2,516,663 (1947).
7. K. Wasa, S. Hayakawa, S. Shooji, and S. Takata, *Jpn. J. Appl. Phys.*, **10**, 1732 (1971).
8. M. Matsuoka, *Jpn. J. Appl. Phys.*, **10**, 736 (1971).
9. T. Minami, *MRS Bull.*, **25**, 38 (2000).
10. R.J. Cava, J.M. Phillips, J. Kwo, G.A. Thomas, R.B. van Dover, S.A. Carter, J.J. Krajewski, W.F. Peck, Jr., J.H. Marshall, and D.H. Rapkine, *Appl. Phys. Lett.*, **64**, 2071 (1994).
11. J.M. Phillips, R.J. Cava, G.A. Thomas, S.A. Carter, J. Kwo, T. Siegrist, J.J. Krajewski, J.H. Marshall, W.F. Peck, Jr., and D.H. Rapkine, *Appl. Phys. Lett.*, **67**, 2246 (1995).
12. D.D. Edwards, T.O. Mason, F. Goutenoire, and K.R. Poeppelmeier, *Appl. Phys. Lett.*, **70**, 1706 (1997).
13. A.J. Freeman, K.R. Poeppelmeier, T.O. Mason, R.P.H. Chang, and T.J. Marks, *MRS Bull.*, **25**, 45 (2000).
14. H. Kawazoe, M. Yasukawa, H. Hyodo, M. Kurita, H. Yanagi, and H. Hosono, *Nature*, **398**, 939 (1997).
15. K. Hayashi, S. Matsuishi, T. Kamiya, M. Hirano, and H. Hosono, *Nature*, **419**, 462 (2002).
16. H. Kawazoe, H. Yanagi, K. Ueda, and H. Hosono, *MRS Bull.*, **25**, 28 (2000).
17. I. Hamberg and C.G. Granqvist, *J. Appl. Phys.*, **60**, R123 (1986).
18. H. Mizoguchi, M. Hirano, S. Fujitsu, T. Takeuchi, K. Ueda, and H. Hosono, *Appl. Phys. Lett.*, **80**, 1207 (2002).
19. T. Moriga, D.D. Edwards, T.O. Mason, G.B. Palmer, and K.R. Poeppelmeier, *J. Am. Ceram. Soc.*, **81**, 1310 (1998).
20. T.J. Coutts, T.O. Mason, J.D. Perkins, and D.S. Ginley, *Electrochem. Soc. Proc.*, **99**(11), 274 (1999).
21. D.R. Kammler, B.J. Harder, N.W. Hrabe, N.M. McDonald, G.B. Gonzalez, D.A. Penake, and T.O. Mason, *J. Am. Ceram. Soc.*, **85**, 2345 (2002).
22. T.O. Mason, G.B. Gonzalez, D.R. Kammler, N. Mansourian-Hadavi, and B.J. Ingram, *Thin Solid Films*, **411**, 106 (2002).
23. R. Asahi, J.R. Babcock, N.L. Edleman, D.R. Kammler, D. Ko, M.A. Lane, A.W. Metz, A. Wang, M. Yan, R.P.H. Chang, V. Dravid, A.J. Freeman, C.R. Kannewurf, T.J. Marks, T.O. Mason, and K.R. Poeppelmeier, *Electrochem. Soc. Proc.*, **2001**(11), 333 (2001).
24. G. Frank and H. Köstlin, *Appl. Phys. A*, **27**, 197 (1982).
25. G.B. Gonzalez, J.B. Cohen, J.-H. Hwang, and T.O. Mason, *J. Appl. Phys.*, **89**, 2550 (2001).
26. R.D. Shannon and C.T. Prewitt, *Acta Cryst. B*, **25**, 925 (1969).
27. D.R. Kammler, T.O. Mason, D.L. Young, and T.J. Coutts, *J. Appl. Phys.*, **90**, 3263 (2001).
28. S.B. Zhang and S.-H. Wei, *Appl. Phys. Lett.*, **80**, 1376 (2002).
29. R.D. Shannon, J.L. Gilson, and R.J. Bouchard, *J. Phys. Chem. Solids*, **38**, 877 (1977).
30. G. Haacke, *Appl. Phys. Lett.*, **28**, 622 (1976).
31. X. Wu, T.J. Coutts, and W.P. Mulligan, *J. Vac. Sci. Technol. A*, **15**, 1057 (1997).
32. H. Ohta, M. Orita, M. Hirano, and H. Hosono, *J. Appl. Phys.*, **91** 3547 (2002).
33. A. Wang, M. Lane, N.L. Edleman, A.W. Metz, M.A. Lane, R. Asahi, V.P. Dravid, C.R. Kannewurf, A.J. Freeman, and T.J. Marks, *Proc. Natl. Acad. Sci.*, **98**, 7113 (2001).
34. F.P. Koffyberg, *Phys. Rev. B*, **13**, 4470 (1976).
35. J. Nell, B.J. Wood, S.E. Dorris, and T.O. Mason, *J. Solid State Chem.*, **82**, 247 (1989).
36. N. Duan, A.W. Sleight, M.K. Jayaray, and J. Tate, *Appl. Phys. Lett.*, **77**, 1325 (2000).
37. B.J. Ingram, T.O. Mason, R. Asahi, K.T. Park, and A.J. Freeman, *Phys. Rev. B*, **64**, 155114 (2001).
38. A.J. Bosman and H.J. van Daal, *Adv. Phys.*, **19**, 1 (1970).
39. Shahriari and Poeppelmeier, unpublished results.
40. H. Katayama-Yoshida, T. Koyanagi, H. Funashima, H. Harima, and A. Yanase, *Solid State Commun.*, **126**, 135 (2003).
41. O. Porat and I. Riess, *Solid State Ionics*, **81**, 29 (1995).
42. B.J. Ingram, Ph.D. Dissertation, Northwestern University, Evanston, IL (2003).
43. Y. Wang and H. Gong, *Chem. Vap. Depos.*, **6**, 285 (2000).
44. B.J. Ingram and T.O. Mason, *J. Electrochem. Soc.*, **150**, E396 (2003).
45. S. Matsuishi, Y. Toda, M. Miyakawa, K. Hayashi, T. Kamiya, M. Hirano, I. Tanaka, and H. Hosono, *Science*, **301**, 626 (2003).